Materials Research Letters

ISSN: (Print) (Online) Journal homepage: https://www.tandfonline.com/loi/tmrl20

Ultrathin epitaxial NbN superconducting films with high upper critical field grown at low temperature

Xiucheng Wei, Pinku Roy, Zihao Yang, Di Zhang, Zihao He, Ping Lu, Olivia Licata, Haiyan Wang, Baishakhi Mazumder, Nag Patibandla, Yong Cao, Hao Zeng, Mingwei Zhu & Quanxi Jia

To cite this article: Xiucheng Wei, Pinku Roy, Zihao Yang, Di Zhang, Zihao He, Ping Lu, Olivia Licata, Haiyan Wang, Baishakhi Mazumder, Nag Patibandla, Yong Cao, Hao Zeng, Mingwei Zhu & Quanxi Jia (2021) Ultrathin epitaxial NbN superconducting films with high upper critical field grown at low temperature, Materials Research Letters, 9:8, 336-342, DOI: 10.1080/21663831.2021.1919934

To link to this article: https://doi.org/10.1080/21663831.2021.1919934

Published online: 29 Apr 2021.

MATER. RES. LETT.
2021, VOL. 9, NO. 8, 336–342
https://doi.org/10.1080/21663831.2021.1919934

MATERIALS RESEARCH LETTERS
Taylor & Francis
Taylor & Francis Group

REPORT

Ultrathin epitaxial NbN superconducting films with high upper critical field grown at low temperature

Xiucheng Wei[a*], Pinku Roy[b*], Zihao Yang[c*], Di Zhang[d], Zihao He[d], Ping Lu[e], Olivia Licata[b], Haiyan Wang[d], Baishakhi Mazumder[b], Nag Patibandla[c], Yong Cao[c], Hao Zeng[a], Mingwei Zhu[c] and Quanxi Jia[b]

[a]Department of Physics, University at Buffalo – the State University of New York, Buffalo, NY, USA; [b]Department of Materials Design and Innovation, University at Buffalo – the State University of New York, Buffalo, NY, USA; [c]Applied Materials, Inc., Santa Clara, CA, USA; [d]School of Materials Engineering, Purdue University, West Lafayette, IN, USA; [e]Sandia National Laboratories, Albuquerque, NM, USA

ABSTRACT

Ultrathin (5–50 nm) epitaxial superconducting niobium nitride (NbN) films were grown on AlN-buffered *c*-plane Al_2O_3 by an industrial scale physical vapor deposition technique at 400°C. Both X-ray diffraction and scanning electron microscopy analysis show high crystallinity of the (111)-oriented NbN films, with a narrow full-width-at-half-maximum of the rocking curve down to 0.030°. The lattice constant decreases with decreasing NbN layer thickness, suggesting lattice strain for films with thicknesses below 20 nm. The superconducting transition temperature, the transition width, the upper critical field, the irreversibility line, and the coherence length are closely correlated to the film thickness.

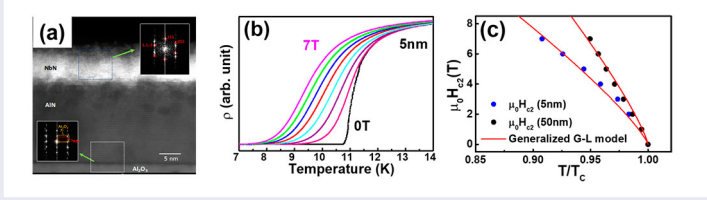

ARTICLE HISTORY
Received 14 April 2021
Accepted 16 April 2021

KEYWORDS
Ultrathin superconducting films; NbN; epitaxial growth; physical vapor deposition

IMPACT STATEMENT

This work realized high quality ultrathin epitaxial NbN films by an industry-scale PVD technology at low substrate temperature, which opens up new opportunities for quantum devices.

Introduction

The ability to grow niobium nitride (NbN) films by different techniques and the relatively higher superconducting transition temperature (T_C) in comparison with other transition metal based superconducting materials have made NbN one of the most widely studied superconducting materials for a range of applications. For example, NbN has emerged as a preferred material for superconducting nanowire single photon detectors (SNSPD) [1–5]. Epitaxial NbN films have also been investigated as the superconducting electrode for Josephson junctions in superconducting quantum interference devices, superconducting qubits, and rapid single flux quantum logic circuits [6–11].

Superconducting NbN thin films have been deposited using different methods including reactive DC/RF magnetron sputtering [12,13], pulsed laser deposition (PLD) [14,15], chemical vapor deposition (CVD) [16,17], molecular beam epitaxy [18,19], atomic layer deposition [20,21], and polymer-assisted deposition (PAD) [22]. Different materials such as MgO [5,23], SiC [24,25], Al_2O_3 [26,27], Si [28,29], and GaAs [3,30] have been used as the substrates for the growth of NbN films. It is known that the superconducting properties (e.g. T_C) of NbN films are sensitive not only to the deposition techniques but also to the growth conditions for a given deposition technique. The substrate materials and the film thickness also play important roles in determining

CONTACT Mingwei Zhu mingwei_zhu@amat.com Applied Materials, Inc., Santa Clara, CA 95054, USA; Quanxi Jia qxjia@buffalo.edu Department of Materials Design and Innovation, University at Buffalo – the State University of New York, Buffalo, NY 14260, USA
*These authors contributed equally to this work.

Supplemental data for this article can be accessed here. https://doi.org/10.1080/21663831.2021.1919934

superconducting properties. For instance, Hazra et al. reported a T_C of around 17 K for 50 nm NbN films grown by high temperature CVD at 1300°C on sapphire and AlN [16]. Zou et al. reported the growth of 18 nm epitaxial NbN film on $SrTiO_3$ with a T_C of 14 K by PAD [22]. Linzen et al. deposited 40 nm NbN films using a plasma-enhanced atomic layer deposition, with a T_C of 13.7 K [31]. The effect of the substrate materials on superconducting properties of NbN films grown by PLD has also been reported, showing a T_C of 13.1 K on MgO and 15.2 K on Al_2O_3 substrates [32]. Furthermore, the Tc of NbN films is extremely sensitive on N concentration. As indicated by Kalal et al., both deficiency or excess of N from equiatomic NbN composition could lead to a reduction in T_C when reactive magnetron sputtering of Nb target at different partial pressure of N_2 was used to grow NbN films [33].

For certain applications, epitaxial NbN film is preferred. Epitaxial NbN film with a thickness of 5 nm grown by DC magnetron sputtering on GaN-buffered sapphire showed a maximum T_C of 13.2 K and an upper critical magnetic field (H_{c2}) greater than 15 T at 0 K [17]. On the other hand, epitaxial NbN films deposited by sputtering on MgO (001) with a film thickness > 50 nm showed H_{c2} around 20 T [34]. To reduce the strain effect of substrate materials on the properties of NbN films, a buffer layer between the NbN film and the substrate has been explored. NbN films with thickness close to 5 nm deposited by magnetron sputtering on *c*- and *M*-plane sapphire substrates with eitehr a $Al_xGa_{1-x}N$ ($x < 20\%$) or an AlN buffer layers respectively showed a maximum T_C of 13.3 K [17,26]. TiN buffer layer on Si has also been investigated where the T_C of NbN film could be improved by about 1–3 K than that on bare Si (100) substrate [29]. A monotonic decrease in T_C with decreasing NbN film thickness is commonly observed when the film thickness is less than 100 nm [13,35,36]. Therefore, it is imperative to investigate the processing-structure-property relationship of the NbN films grown by a particular deposition technique, with the purpose of optimizing their performance for specific applications.

In this work, we show that wafer scale and high crystallinity superconducting NbN thin films (5–50 nm) can be epitaxially grown on AlN buffered (20 nm) *c*-plane Al_2O_3 by sputtering at a substrate temperature of 400°C. The epitaxial NbN films exhibit an in-plane strain when the film thickness is less than 20 nm. The strained ultrathin (~ 5 nm) epitaxial NbN film shows an upper critical field of 36 ± 2 T and an irreversibility line of 16 ± 1 T at 4.2 K, and a coherence length of 2.542 ± 0.002 nm.

Materials and methods

The AlN and NbN layered structures were deposited on 2-inch *c*-plane sapphire in two separate Applied Materials' 300-mm Impulse™ physical vapor deposition (PVD) chambers. Both AlN buffer layer and NbN layers were deposited via reactive ion sputtering from Al and Nb targets respectively in Ar and N_2 ambient at a substrate temperature of 400°C. The crystal structure and microstructure of NbN films with varying thickness were analyzed by x-ray analysis and scanning TEM (STEM) using high-angle annular dark-field (HAADF) detector. The details of the processing parameters to grow the films, the x-ray analysis, TEM characterization, and superconducting property measurement can be found from the Supplementary Information.

Results and discussion

The superconducting properties of the epitaxial NbN films depend strongly on their crystalline quality. The surface and interface also play important roles in determining the superconducting properties of ultrathin NbN films. Therefore, it is essential to fully characterize the structure of the NbN films. The film orientation with respect to the single crystal *c*-plane Al_2O_3, phase purity, crystallinity, and interface roughness were characterized by x-ray diffraction including θ-2θ scans, ω-rocking curves, ϕ-scans, and surface reflectivity measurements. Figure 1 shows the x-ray θ-2θ scans of the films with different film thicknesses at 2θ angle around (111) diffraction of the cubic NbN. The θ-2θ scans over a wide range of 2θ angles is shown in the Figure S1 (Supplementary Information). It is noted that the (111) diffraction peak shifts to the smaller angle with increasing the film thickness. Inset in Figure 1 shows the full-width-at-half-maximum (FWHM) of the ω-rocking curve of the (111) diffraction and the *a*-axis lattice parameter of the NbN thin films with different film thicknesses, where the lattice parameter is calculated from the (002) diffraction. As can be seen from the thickness dependent lattice parameter of the NbN films shown in the inset of Figure 1, the lattice parameter of NbN remains nearly constant at 4.392 Å for films with a thickness ranging from 50 to 20 nm, and then decreases monotonically to 4.365 Å (5 nm). This suggests an *a*-axis lattice strain of up to 1% (considering the lattice constant of bulk NbN as 4.39 Å) for the 5 nm NbN film. This can be understood by considering that the lattice constant of Al_2O_3 is 4.785 Å. The change of lattice parameter with film thickness is further confirmed by analyzing the selected area electron

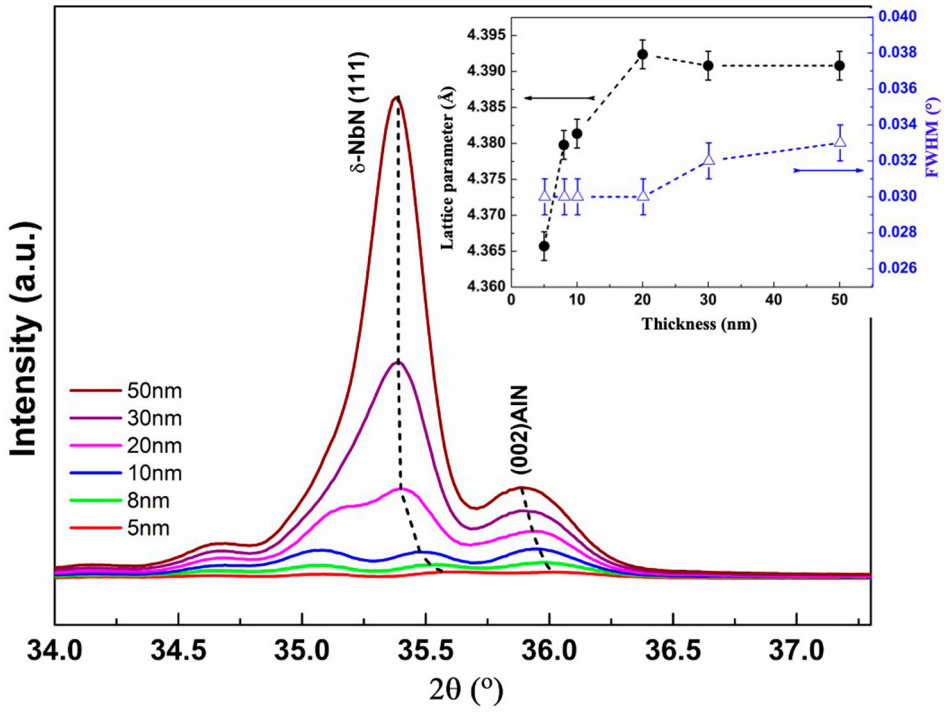

Figure 1. X-ray θ-2θ scans of the NbN films with different film thicknesses. Inset shows NbN film thickness dependent lattice parameter and full width at half maximum of ω-rocking curve of the NbN (111) diffraction.

diffraction (SAED) patterns (see Figure S2 in Supplementary Information). Using Al_2O_3 (006) plane spacing as the reference, the lattice parameter evaluated from SAED patterns is 4.370 Å and 4.390 Å for 5 and 50 nm NbN films, respectively. Both (001)-oriented AlN and (111)-oriented NbN films are compressively strained in-the-plane based on the crystal structure and the epitaxial relationship between the film and the substrate. It is noted that the 5 nm NbN film may not be in coherent strain due to the extra interface roughness resulted from the AlN buffer layer as shown in Figure 2. The FWHM of the rocking curve as shown in the inset of Figure 1, on the other hand, remains almost constant with a value around 0.030° ~ 0.033° when the NbN film thickness changes from 5 to 50 nm. Such a narrow rocking curve clearly indicates that high crystallinity (111)-oriented NbN films could be deposited by a low temperature sputtering technique.

The growth of highly crystalline epitaxial NbN films at a low substrate temperature by sputtering is further confirmed by the ϕ-scan of the (002) NbN film and the (116) Al_2O_3 (see Figure S3 in Supplemental Information). The (111) NbN basal plane is well aligned with the substrate as illustrated by the six diffraction peaks 60° apart from each other. Based on the θ-2θ scan of NbN/AlN/Al_2O_3 heterostructure and the ϕ-scans of the (002) NbN and the (116) Al_2O_3, the overall epitaxial relationship between the NbN and c-plane Al_2O_3 can be described as $(111)_{NbN}||(001)_{AlN}||(001)_{Al2O3}$ and $[1\bar{1}0]_{NbN}||[100]_{AlN}||[120]_{Al2O3}$. We suggest that the AlN buffer layer plays a critical role in the epitaxial growth of NbN on c-plane Al_2O_3 since the lattice mismatch along the [100] AlN ($a_{AlN} = 0.311$ nm) and [1$\bar{1}$0] NbN ($\sqrt{2}a_{NbN}/2 = 0.310$ nm) is less than 0.3%.

Figure 2 shows the STEM-HAADF image with corresponding energy dispersive x-ray spectroscopy (EDS) maps of the NbN film (5 nm) on AlN-buffered c-plane Al_2O_3, obtained when the Al_2O_3 was aligned along $<120>$ zone axis. The high-resolution HAADF image shown in Figure 2a illustrates a sharp interface between the AlN buffer layer and Al_2O_3 substrate. The interface between the NbN and AlN very much follows the morphology of the AlN buffer layer. The crystallographic orientation relationship between the films and substrate can be identified by observing the Fourier-filtered transform (FFT) patterns from the AlN/Al_2O_3 interface and the NbN film (shown in the insets of Figure 2a). The overall epitaxial relationship of NbN on AlN-buffered c-plane Al_2O_3 matches with the x-ray diffraction measurement. It should be noted that the NbN film is expected to grow in two equivalent domains related by 180° rotation about the vertical axis or by the twin relationship on (111) planes, considering the symmetry of cubic NbN (111) on hexagonal AlN (001) plane and the orientation relationship between the two phases (NbN and AlN). The twinning structure in NbN is indeed observed in

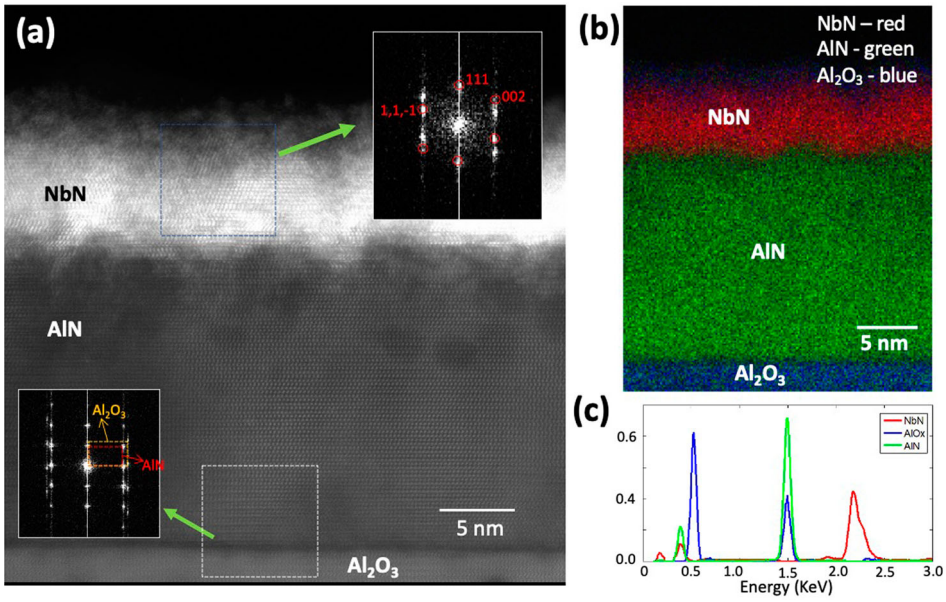

Figure 2. STEM analysis of NbN film (5 nm) on AlN-buffered *c*-plane Al_2O_3. (a) HAADF image of the layered structure NbN/AlN/Al_2O_3. Insets show the FFT patterns from the AlN/Al_2O_3 interface (bottom square region) and the NbN film (top square region); (b) EDS maps of the chemical components of layered structure; (c) EDS spectrum of each component.

the FFT pattern shown in the inset, in which the spots are related by 180° rotation about the vertical axis. The EDS maps shown in Figure 2b are displayed according to three principal components with NbN in red, AlN in green and Al_2O_3 in blue, respectively, obtained by the principal component analysis of the EDS spectral imaging. Figure 2c shows the respective spectrum for each component, verifying the three phases.

Given the heteroepitaxial nature of the NbN films, it is important to explore the thickness dependent superconducting properties of the films. Figure 3 shows the thickness dependent T_C of the NbN films, where T_C is determined from the peak position of the dR/dT *vs*. T plot and R is the resistance of the film. As can be seen from Figure 3, the T_C decreases linearly from 15.3 K (50 nm film) to 11.2 K (5 nm film) with the inverse film thickness, 1/*d*, where *d* is the film thickness. Using Simonin model [37] $(d) = T_{C,bulk}(1 - d_C/d)$, we find that the critical thickness d_C where the T_C of the film disappears, is 1.38 nm. The suppression of T_C with decreasing thickness can be attributed to increase in lattice disorder of the NbN film [38]. It is further noted that the films show sharp transition width (ΔT_C) (derived from FWHM value in dR/dT *vs*. T plot) from 0.4 to 0.06 K by increasing NbN thickness.

Thickness dependent T_C has been widely reported for superconducting materials. In particular, lattice strain can play an important role in determining T_C of very thin epitaxial superconducting films. It is widely accepted that electron-phonon coupling can be much enhanced by biaxial strain, and thus a much higher T_C can be induced

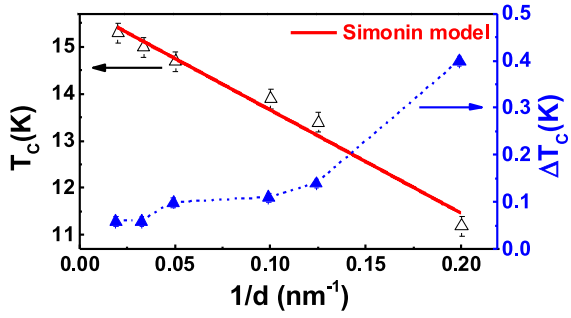

Figure 3. NbN film thickness dependent T_C and transition width, ΔT_C. The T_C decreases linearly with increasing 1/*d*. The ΔT_C, on the other hand, increases with 1/*d*.

in the biaxial strained films. For example, it has been reported that in-plane compressive strain can enhance the T_C of $SrTiO_3$ by up to a factor of two, resulting from the strain-induced modification of phonon modes [39]. More study further revealed that both strain and disorder could control T_C [40,41]. A systematic increase of T_C with epitaxial tensile strain in MgB_2 films has also been reported, resulted from the softening of the bond-stretching phonon mode [42]. On the other hand, it has been reported that strain can cause significant sub-lattice distortion in the lattice structure of Nb_3Sn, and lead to reduction of its superconducting properties, primarily due to changes in the density of states at Fermi surface with a lesser contribution due to change in the phonon spectrum [43]. For superconducting NbN, the situation can be more complex since the lattice parameter can

increase continuously with an increase in N concentration due to an expansion and distortion in NbN lattice caused by the interstitial incorporation of N atoms [33]. It has been reported that the lowest Raman peak in δ-NbN due to acoustic phonons shifts to higher frequencies with increasing deviation from stoichiometry [44]. This could lead to a sharp decrease in T_C. The thickness dependent T_C of our ultrathin NbN films may not result from the increase in N concentration and/or deviation from the ideal stoichiometry. As shown in Figure 1, the lattice parameter decreases with decreasing film thickness. Our NbN films were deposited under the same processing conditions except for the film thickness. The high crystallinity epitaxial NbN films may suggest that the surface, the interface, and the grain size can all affect the T_C. Accordingly, the grain size, calculated based on the Scherrer's equation from x-ray diffraction, was found to be around 15 and 38 nm for NbN films with thickness of 5 and 50 nm, respectively. Furthermore, it is well known that the T_C of a given superconductor decreases significantly when the film thickness is comparable with the coherence length of the superconductor. Given that T_C is closely related to the phonon spectrum, the electronic density of state, the electron-phonon coupling, and electron-electron interaction, more detailed study is necessary to deconvolute the fundamental mechanisms that control the T_C at a film thickness comparable to the superconducting coherence length.

The superconducting transition width, ΔT_C, at different applied magnetic fields is directly related to the upper critical field (H_{c2}) and irreversibility field (H_{irr}). Figure 4(a) shows ΔT_C as a function of external magnetic field (H) perpendicular to the film surface, where the film thickness is 5 and 50 nm, respectively. It can be seen that T_C shifts to lower temperatures with increasing H, as shown in Figure 4(b), regardless of the film thickness, where the field dependent resistivity vs. temperature characteristics of the 50 nm thick film is shown in Figure S4 (Supplementary Information). Importantly, ΔT_C increases with H for both films as shown in Figure 4(a). For the thinner film (5 nm), ΔT_C rises from $\sim$1.5 to $\sim$3 K as the magnetic field increases from 0 to 7 T. On the other hand, the variation of ΔT_C is much smaller and changes from $\sim$0.15 to $\sim$0.5 K for the thicker film (50 nm) when magnetic field increases from 0 to 7 T.

Both the upper critical field H_{c2} (at which the superconductor becomes normal) and the irreversibility field H_{irr} (at which the superconductor ceases to carry supercurrent) are a strong function of film thickness. The H_{c2} and H_{irr} at a given temperature are defined as the fields at which the resistance of the superconducting film is 90% and 10% of the normal state resistance, respectively. Figure 4(c) and (d) show the normalized temperature, T/T_C, dependence of H_{c2} and H_{irr} for both 5 and 50 nm NbN films, respectively. To

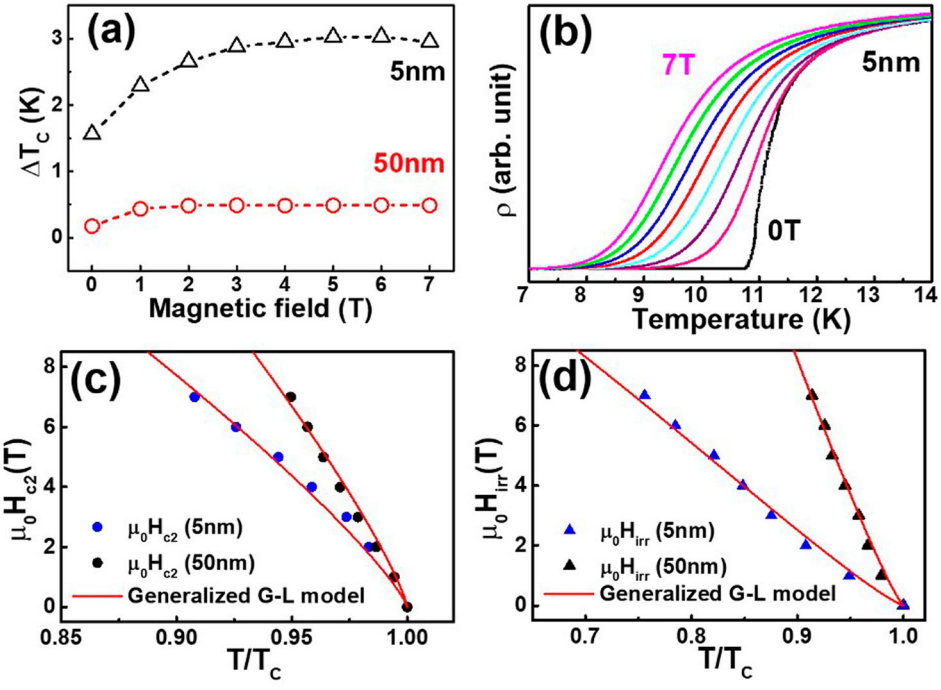

Figure 4. Magnetic field dependent superconducting properties. (a) Superconducting transition width, ΔT_C, as a function of field. (b) Resistivity vs. temperature characteristics at different fields for a 5 nm NbN film. (c) H_{c2} and (d) H_{irr} as a function of normalized temperature of both 5 and 50 nm NbN films.

extrapolate $\mu_0 H_{c2}$ and $\mu_0 H_{irr}$ at liquid helium temperature, the generalized Ginzburg-Landau (G-L) model [45] is used: $H_{c2}(T) = H_{c2}(0)[1-(T/T_c)^a]^b$ and $H_{irr}(T) = H_{irr}(0)[1-(T/T_c)^a]^b$. The generalized G-L model can best fit our data with $a = 1.0$, and $b = 0.82$ for H_{c2}(T) and $a = 1.8$, and $b = 1.18$ for H_{irr}(T). The $\mu_0 H_{c2}$ (4.2 K) extracted from the plots is 36 ± 2 T and 60 ± 2 T for NbN films of 5 and 50 nm, respectively, while $\mu_0 H_{irr}$ (4.2 K) is 16 ± 1 T and 57 ± 1 T for NbN films of 5 and 50 nm, respectively. From the G-L theory, the effective coherence length at 0 K can be described by $\xi(0) = \sqrt{\phi_0/[2\pi H_{c2}(0)]}$, where $\phi_0 = 2.07 \times 10^{-7} Gcm^2$ is the magnetic flux quantum. The coherence length of the epitaxial NbN films on AlN-buffered *c*-plane Al_2O_3 is $\xi(0\ \text{K}) = 2.542 \pm 0.002$ nm and 2.055 ± 0.001 nm for NbN films of 5 and 50 nm, respectively. Apparently, increasing film thickness can increase $\mu_0 H_{c2}$, and thus decrease the coherence length.

Conclusion

We have grown high-quality ultrathin epitaxial superconducting NbN films on *c*-plane Al_2O_3 using sputtering at a substrate temperature of 400°C, where AlN is used as a buffer layer. Both x-ray diffraction and transmission electron microscopy studies reveal that the (111)-oriented NbN films are of high crystallinity. Epitaxial NbN film with a thickness less than 20 nm is under strain. For an ultrathin NbN film (5 nm), the lattice strain is about 1%. Our experimental results also indicate that the T_C of (111)-oriented epitaxial NbN films decreases with the film thickness, where the T_C is suggested to disappear at a film thickness around 1.4 nm. A 5 nm NbN film exhibits a T_C of 11.2 K, an upper critical field of 36 ± 2 T, an irreversibility line of 16 ± 1 T at 4.2 K, and a coherence length of 2.542 ± 0.002 nm. This demonstrates the feasibility of producing high-performance epitaxial superconducting films for quantum devices using an industry-scale PVD technology.

Acknowledgements

The work at University at Buffalo (UB) was partially supported by both the SUNY Applied Materials Research Institute, a strategic alliance between the State University of New York (SUNY) and Applied Materials, Inc. and the UB's New York State Center of Excellence in Materials Informatics through the Co-Funded Projects between UB faulty and industry collaborators. D.Z. and H.W. acknowledge the support by U.S. NSF under DMR-2016453 and DMR-1565822. Sandia National Laboratories is a multimission laboratory managed and operated by National Technology and Engineering Solutions of Sandia, LLC., a wholly owned subsidiary of Honeywell International, Inc., for the U.S. Department of Energy's National Nuclear Security Administration under contract DE-NA0003525. This paper describes objective technical results and analysis. Any subjective views or opinions that might be expressed in the paper do not necessarily represent the views of the U.S. Department of Energy or the United States Government.

Disclosure statement

No potential conflict of interest was reported by the author(s).

Funding

The work at University at Buffalo (UB) was partially supported by both the SUNY Applied Materials Research Institute and the UB's New York State Center of Excellence in Materials Informatics through the Co-Funded Projects. D.Z. and H.W. acknowledge the support by U.S. NSF under DMR-2016453 and DMR-1565822.

ORCID

Haiyan Wang http://orcid.org/0000-0002-7397-1209
Hao Zeng http://orcid.org/0000-0002-6692-6725
Quanxi Jia http://orcid.org/0000-0002-7683-5202

References

[1] Zhang W, You L, Li H, et al. NbN superconducting nanowire single photon detector with efficiency over 90% at 1550 nm wavelength operational at compact cryocooler temperature. Sci China Phys Mech Astron. 2017;60:120314.
[2] Gol'tsman G, Okunev O, Chulkova G, et al. Fabrication and properties of an ultrafast NbN hot-electron single-photon detector. IEEE Trans Appl Supercond. 2001;11:574–577.
[3] Schmidt E, Ilin K, Siegel M. AlN-buffered superconducting NbN nanowire single-photon detector on GaAs. IEEE Trans Appl Supercond. 2017;27:1–5.
[4] Lipatov A, Okunev O, Smirnov K, et al. An ultrafast NbN hot-electron single-photon detector for electronic applications. Supercond Sci Technol. 2002;15:1689–1692.
[5] Miki S, Fujiwara M, Sasaki M, et al. NbN superconducting single-photon detectors prepared on single-crystal MgO substrates. IEEE Trans Appl Supercond. 2007;17:285–288.
[6] Liu Q, et al. All-NbN DC-SQUID magnetometer based on NbN/AlN/NbN Josephson junctions. IEEE Trans Appl Supercond. 2017;27:1–4.
[7] Shoji A. Fabrication of all-NbN Josephson tunnel junctions using single crystal NbN films for the base electrodes. IEEE Trans Magn. 1991;27:3184–3187.
[8] Nakamura Y, Terai H, Inomata K, et al. Superconducting qubits consisting of epitaxially grown NbN/AlN/NbN Josephson junctions. Appl Phys Lett. 2011;99:212502.
[9] Terai H, Makise K, Wang Z. Operation of single-flux-quantum logic cells based on all-NbN integrated circuit technology. In *2013 IEEE 14th International Superconductive Electronics Conference (ISEC)* 1–3 (2013). doi:10.1109/ISEC.2013.6604278.
[10] Radparvar M. A niobium nitride-based analog to digital converter using rapid single flux quantum logic operating at 9.5 K. IEEE Trans Appl Supercond. 1994;4:92–96.

[11] Kaul AB, Whiteley SR, Van Duzer T, et al. Internally shunted sputtered NbN Josephson junctions with a TaNx barrier for nonlatching logic applications. Appl Phys Lett. 2001;78:99–101.
[12] Mondal M, Chand M, Kamlapure A, et al. Phase diagram and upper critical field of homogeneously disordered epitaxial 3-dimensional NbN films. J Supercond Nov Magn. 2011;24:341–344.
[13] Reithmaier G, Senf J, Lichtmannecker S, et al. Optimisation of NbN thin films on GaAs substrates for *in-situ* single photon detection in structured photonic devices. J Appl Phys. 2013;113:143507.
[14] Ufuktepe Y, Farha AH, Kimura SI, et al. Superconducting niobium nitride thin films by reactive pulsed laser deposition. Thin Solid Films. 2013;545:601–607.
[15] Treece RE, Horwitz JS, Claassen JH, et al. Pulsed laser deposition of high-quality NbN thin films. Appl Phys Lett. 1994;65:2860–2862.
[16] Hazra D, Tsavdaris N, Jebari S, et al. Superconducting properties of very high quality NbN thin films grown by high temperature chemical vapor deposition. Supercond Sci Technol. 2016;29:105011.
[17] Krause S, Meledin D, Desmaris V, et al. Epitaxial growth of ultra-thin NbN films on $Al_xGa_{1-x}N$ buffer-layers. Supercond Sci Technol. 2014;27:065009.
[18] Yan R, Khalsa G, Vishwanath S, et al. Gan/NbN epitaxial semiconductor/superconductor heterostructures. Nature. 2018;555:183–189.
[19] Wang G-Y, Zhu Z, Yang X-Y, et al. Atomically flat superconducting NbN thin films grown on $SrTiO_3$ (111) by plasma-assisted MBE. APL Mater. 2017;5:126107.
[20] Ziegler M, Fritzsch L, Day J, et al. Superconducting niobium nitride thin films deposited by metal organic plasma-enhanced atomic layer deposition. Supercond Sci Technol. 2013;26:025008.
[21] Ukibe M, Fujii G. Superconducting characteristics of NbN films deposited by atomic layer deposition. IEEE Trans Appl Supercond. 2017;27:1–4.
[22] Zou G, Jain M, Zhou H, et al. Ultrathin epitaxial superconducting niobium nitride films grown by a chemical solution technique. Chem Commun. 2008;45:6022–6024. doi:10.1039/B815066D.
[23] Boffa V, Gambardella U, Marotta V, et al. Nbn superconducting thin films grown by pulsed laser ablation. Appl Surf Sci. 1996;106:361–364.
[24] Dochev D, Desmaris V, Pavolotsky A, et al. Growth and characterization of epitaxial ultra-thin NbN films on 3C-SiC/Si substrate for terahertz applications. Supercond Sci Technol. 2011;24:035016.
[25] Chang HW, Wang CL, Huang YR, et al. Growth and characterization of few unit-cell NbN superconducting films on 3C-SiC/Si substrate. Supercond Sci Technol. 2017;30:115010.
[26] de Lamaestre RE, Odier P, Bellet-Amalric E, et al. High quality ultrathin NbN layers on sapphire for superconducting single photon detectors. J Phys Conf Ser. 2008;97:012046.
[27] Espiau de Lamaëstre R, Odier P, Villégier J-C. Microstructure of NbN epitaxial ultrathin films grown on A-, M-, and R-plane sapphire. Appl Phys Lett. 2007;91:232501.
[28] Ilin K, Schneider R, Gerthsen D, et al. Ultra-thin NbN films on Si: crystalline and superconducting properties. J Phys Conf Ser. 2008;97:012045.
[29] Zhang JJ, Su X, Zhang L, et al. Improvement of the superconducting properties of NbN thin film on single-crystal silicon substrate by using a TiN buffer layer. Supercond Sci Technol. 2013;26:045010.
[30] Marsili F, Gaggero A, Li LH, et al. High quality superconducting NbN thin films on GaAs. Supercond Sci Technol. 2009;22:095013.
[31] Linzen S, Ziegler M, Astafiev OV, et al. Structural and electrical properties of ultrathin niobium nitride films grown by atomic layer deposition. Supercond Sci Technol. 2017;30:035010.
[32] Volkov S, et al. Superconducting properties of very high quality NbN thin films grown by pulsed laser deposition. J Electr Eng. 2019;70:89–94.
[33] Kalal S, Gupta M, Rawat R. N concentration effects on structure and superconductivity of NbN thin films. J Alloys Compounds. 2021;851:155925.
[34] Jesudasan J, Mondal M, Chand M, et al. Upper critical field and coherence length of homogenously disordered epitaxial 3-dimensional NbN films. AIP Conf Proc. 2011;1349:923–924.
[35] Wang Z, Kawakami A, Uzawa Y, et al. Superconducting properties and crystal structures of single-crystal niobium nitride thin films deposited at ambient substrate temperature. J Appl Phys. 1996;79:7837–7842.
[36] Shiino T, Shiba S, Sakai N, et al. Improvement of the critical temperature of superconducting NbTiN and NbN thin films using the AlN buffer layer. Supercond Sci Technol. 2010;23:045004.
[37] Simonin J. Surface term in the superconductive Ginzburg-Landau free energy: application to thin films. Phys Rev B. 1986;33:7830–7832.
[38] Narlikar AV, Ekbote SN.Superconductivity and superconducting materials. New Delhi: South Asian Publishers; 1983.
[39] Ahadi K, Galletti L, Li Y, et al. Enhancing superconductivity in $SrTiO_3$ films with strain. Sci Adv. 2019;5:eaaw0120.
[40] Russell R, Ratcliff N, Ahadi K, et al. Ferroelectric enhancement of superconductivity in compressively strained $SrTiO_3$ films. Phys Rev Mater. 2019;3:091401(R).
[41] Salmani-Rezaie S, Ahadi K, Stemmer S. Polar nanodomains in a ferroelectric superconductor. Nano Lett. 2020;20:6542–6547.
[42] Pogrebnyakov AV, Redwing JM, Raghavan S, et al. Enhancement of the superconducting transition temperature of MgB_2 by a strain-induced bond-stretching mode softening. Phys Rev Lett. 2004;93:147006.
[43] Godeke A, Hellman F, Kate H, et al. Fundamental origin of the large impact of strain on superconducting Nb_3Sn. Supercond Sci Technol. 2018;31:105011.
[44] Kaiser R, Spengler W, Schicktanz S, et al. Raman spectra and superconductivity of various phases of a high-Tc superconductor: NbN. Physica Status Solidi (b). 1978;87:565–573.
[45] Zehetmayer M, Weber HW. Experimental evidence for a two-band superconducting state of $NbSe_2$ single crystals. Phys Rev B. 2010;82:014524.